Journal of Molecular Structure 1109 (2016) 131–138

Contents lists available at ScienceDirect

Journal of Molecular Structure

journal homepage: http://www.elsevier.com/locate/molstruc

Spectroscopic investigations and molecular docking study of 3-(1*H*-imidazol-1-yl)-1-phenylpropan-1-one, a potential precursor to bioactive agents

Monirah A. Al-Alshaikh [a], Sheena Mary Y [b], C.Yohannan Panicker [b, *], Mohamed I. Attia [c, d], Ali A. El-Emam [c], C.Van Alsenoy [e]

[a] Department of Chemistry, College of Sciences, King Saud University, Riyadh 11451, Saudi Arabia
[b] Department of Physics, Fatima Mata National College, Kollam, Kerala, India
[c] Department of Pharmaceutical Chemistry, College of Pharmacy, King Saud University, Riyadh 11451, Saudi Arabia
[d] Medicinal and Pharmaceutical Chemistry Department, Pharmaceutical and Drug Industries Research Division, National Research Centre, Dokki, Giza 12622, Egypt
[e] Department of Chemistry, University of Antwerp, Groenenborgerlaan 171, Antwerp B-2020, Belgium

ARTICLE INFO

Article history:
Received 14 October 2015
Received in revised form
27 December 2015
Accepted 28 December 2015
Available online 30 December 2015

Keywords:
DFT
Imidazole
Hyperpolarizability
Molecular docking
NBO

ABSTRACT

The optimized molecular structure, vibrational wavenumbers, corresponding vibrational assignments of 3-(1*H*-imidazol-1-yl)-1-phenylpropan-1-one have been investigated theoretically and experimentally. The calculated geometrical parameters of the title compound are in agreement with the reported XRD data. The HOMO and LUMO analysis is used to determine the charge transfer within the molecule. The stability of the molecule arising from hyper-conjugative interaction and charge delocalization has been analyzed using NBO analysis. Molecular electrostatic potential was performed by the DFT method and from the MEP plot, it is evident that the negative charge covers the carbonyl group and the nitrogen atom N_3 of the imidazole ring and the positive region is over the remaining portions of the molecule. The first and second hyperpolarizabilities are calculated and the first hyperpolarizability of the title compound is 16.99 times that of standard NLO material urea and the title compound and its derivatives are good object for further studies in nonlinear optics. The docked ligand title compound forms a stable complex with *plasmodium falciparum* and gives a binding affinity value of −5.5 kcal/mol and the preliminary results suggest that the compound might exhibit antimalarial activity against *plasmodium falciparum*.

1. Introduction

An increased incidence of both community-acquired and nosocomial invasive fungal infections has been witnessed over the past few decades. Nosocomial invasive and systemic fungal infections are considered one of the major causes of morbidity and mortality, particularly in patients with weakened or compromised immune systems such as patients with cancer or AIDS and in organ transplant cases [1,2]. In addition, *Candida* species represent the main agent for nosocomial fungal infections worldwide with *Candida albicans* being the cause for the majority of invasive candidiases with about 30–40% of mortality [3]. Antifungal agents having azole moiety constitute the mainstay for treatment of fungal infections owing to their safety profile and good therapeutic index [4]. Azoles are nitrogen-containing five membered heterocyclic compounds with electron-rich property. Thereby, they can easily bind with the enzymes and receptors in organisms through weak interactions such as coordination bonds, hydrogen bonds, ion-dipole, π-π stacking as well as van der Waals force *etc*., leading to diverse biological activities. The antifungal activity of azoles is attributed to the co-ordination binding of the heterocyclic nitrogen atom to the heme iron atom in the binding site of 14α-demethylase enzyme causing depletion of ergosterol. The ability of azoles to interact with the heme of many host cytochrome P450 enzymes, particularly mammalian CYP3A4, is the reason for the appearance of systemic azole toxicity [5,6]. Imidazole is a 1,3-diaza five membered heterocyclic azole. A plethora of imidazole-bearing antifungals have been used to treat fungal diseases due to their

* Corresponding author.
E-mail address: cyphyp@rediffmail.com (C.Yohannan Panicker).

http://dx.doi.org/10.1016/j.molstruc.2015.12.075
0022-2860/

low toxicity and broad antimicrobial spectrum including yeasts and fungal strains. Accordingly, researchers were encouraged to develop new antifungal agents incorporating imidazole moiety [7]. N-Alkylated imidazole moiety is a common feature in many antifungal agents used in clinics, namely clotrimazole, miconazole, econazole and ketoconazole [8]. Therefore, much more attention has been paid in the investigations of such kind of antifungal imidazoles. The clinically available antifungal agents suffer from the development of drug resistance, undesirable side effects and high risk of toxicity [9]. This necessitates continuous efforts to develop new potent antifungal agents with fewer side effects in order to address these therapeutic issues. The title compound is an azole-containing compound bearing *N*-alkylated imidazole moiety and is the building block of a number of anti-*Candida* agents [10–12].

Spectroscopic studies of certain imidazole derivatives are already reported [13–15]. The present work describes the natural bond orbital analysis, molecular frontier orbital analysis, nonlinear optical properties and molecular potential surface study of the title compound. The experimentally observed infrared and Raman bands have been assigned with the help of the calculated vibrational frequencies and potential energy distribution analysis. In addition, a molecular docking study of the title compound is also reported due to the diverse biological activities of the imidazole derivatives [16–18].

2. Experimental details

A pure sample of the title compound was prepared via the reaction of 3-(dimethylamino)-1-phenylpropan-1-one hydrochloride with imidazole in water following the previously reported procedure of Attia et al. [19].

The FT-IR spectrum (Fig. 1) was recorded using KBr pellets on a DR/Jasco FT-IR 6300 spectrometer with a spectral resolution of 2 cm^{-1}. The FT-Raman spectrum (Fig. 2) was obtained on a Bruker RFS 100/s, Germany, and for excitation of the spectrum, the emission of Nd:YAG laser was used, excitation wavelength was 1064 nm, maximal power was 150 mW and measurement was carried out on solid sample.

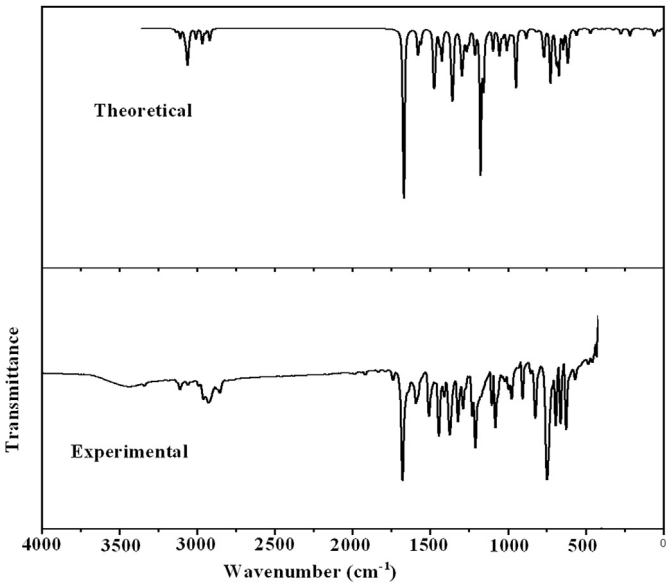

Fig. 1. FT-IR spectrum of 3-(1*H*-imidazol-1-yl)-1-phenylpropan-1-one.

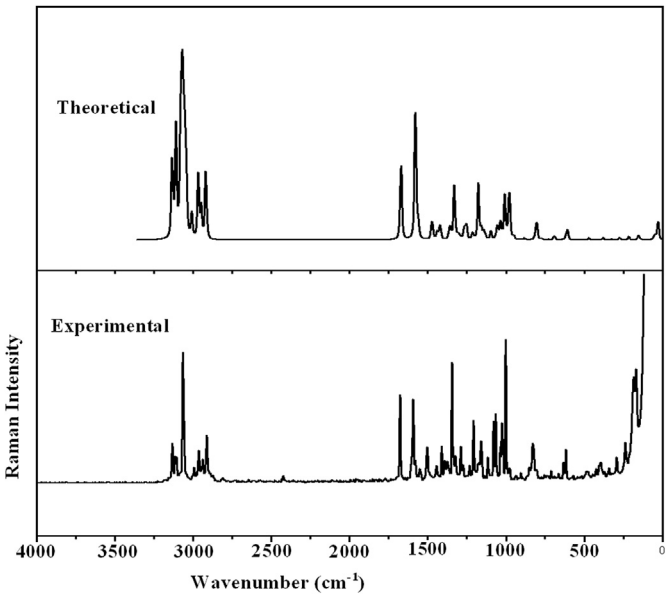

Fig. 2. FT-Raman spectrum of 3-(1*H*-imidazol-1-yl)-1-phenylpropan-1-one.

3. Computational details

All calculations have been performed with the Gaussian09 software [20] using the density functional theoretical method [21]. The theoretical calculations were performed with the hybrid B3LYP functional, i.e. a combination of the Becke's three parameter exchange functional [22] and Lee-Yang-Parr correlation functional [23,24]. The DFT calculations were reported to provide excellent vibrational frequencies of organic compounds if the calculated frequencies are scaled to compensate for the approximate treatment of electron correlation, for basis set deficiencies and for the anharmonicity [25]. The optimized structure parameters (Fig. 3) and frequencies were calculated using the DFT/B3LYP method at $6-311++G(d)$ (5D, 7F) basis set level. The absence of imaginary frequencies confirmed that the stationary points correspond to minima on the potential energy surface. The vibrational assignments of the title compound are done with the help of Guassview program [26] and GAR2PED software [27]. The optimized geometrical parameters with the XRD data are given in Table 1.

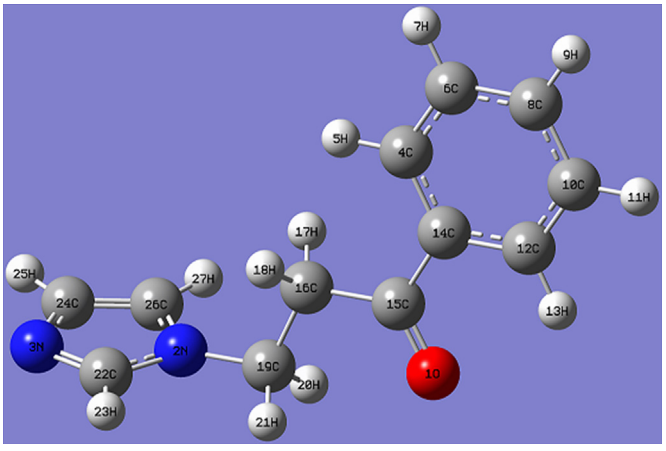

Fig. 3. Optimized geometry of 3-(1*H*-imidazol-1-yl)-1-phenylpropan-1-one.

Table 1
Optimized geometrical parameters of the title compound.

Bond lengths (DFT/XRD) (Å)			
O1–C15	1.2179/1.2152	N2–C19	1.4587/1.4576
N2–C22	1.3672/1.3445	N2–C26	1.3812/1.3612
N3–C22	1.3141/1.3098	N3–C24	1.3747/1.3622
C4–H5	1.0841/0.9300	C4–C6	1.3927/1.3842
C4–C14	1.4018/1.3909	C6–H7	1.0850/0.9300
C6–C8	1.3938/1.3832	C8–H9	1.0854/0.9300
C8–C10	1.3963/1.3762	C10–H11	1.0851/0.9300
C10–C12	1.3892/1.3812	C12–H13	1.0838/0.9300
C12–C14	1.4026/1.3937	C14–C15	1.4976/1.4960
C15–C16	1.5242/1.5052	C16–H17	1.0957/0.9700
C16–H18	1.0958/0.9700	C16–C19	1.5312/1.5142
C19–H20	1.0908/0.9700	C19–H21	1.0903/0.9700
C22–H23	1.0812/0.9300	C24–H25	1.0801/0.9300
C24–C26	1.3718/1.3493	C26–H27	1.0790/0.9300
Bond angles (DFT/XRD) (°)			
C19–N2–C22	126.8/127.0	C19–N2–C26	126.9/126.9
C22–N2–C26	106.2/106.0	C22–N3–C24	105.2/104.1
H5–C4–C6	119.0/119.8	H5–C4–C14	120.6/119.8
C6–C4–C14	120.4/120.5	C4–C6–H7	119.9/119.9
C4–C6–C8	120.0/120.2	H7–C6–C8	120.1/119.9
C6–C8–H9	120.0/120.1	C6–C8–C10	120.0/119.8
H9–C8–C10	120.0/120.1	C8–C10–H11	120.0/119.9
C8–C10–C12	120.0/120.2	H11–C10–C12	119.9/119.9
C10–C12–H13	121.0/119.7	C10–C12–C14	120.5/120.7
H13–C12–C14	118.5/119.7	C4–C14–C12	119.1/118.6
C4–C14–C15	122.7/122.5	C12–C14–C15	118.3/118.9
O1–C15–C14	121.0/120.6	O1–C15–C16	120.2/120.8
C14–C15–C16	118.7/118.6	C15–C16–H17	109.2/109.0
C15–C16–H18	109.4/109.0	C15–C16–C19	112.4/113.0
H17–C16–H18	105.6/107.8	H17–C16–C19	110.1/109.0
H18–C16–C19	109.8/109.0	N2–C19–C16	112.1/111.4
N2–C19–H20	109.0/109.3	N2–C19–H21	108.1/109.3
C16–C19–H20	110.7/109.3	C16–C19–H21	110.4/109.3
H20–C19–H21	106.4/108.0	N2–C22–N3	112.4/112.9
N2–C22–H23	121.9/123.6	N3–C22–H23	125.7/123.6
N3–C24–H25	121.4/124.6	N3–C24–C26	110.5/110.9
H25–C24–C26	128.1/124.6	N2–C26–C24	105.8/106.1
N2–C26–H27	121.9/126.9	C24–C26–H27	132.3/126.9
Torsion angles (DFT/XRD) (°)			
C14–C4C6C8	0.0/0.3	C4–C6–C8–C10	0.0/-1.3
C6–C8–C10–C12	−0.0/0.8	C8–C10–C12–C14	0.0/0.8
C6–C4–C14–C12	−0.0/1.2	C6–C4–C14–C15	179.9/178.0
C10–C12–C14–C4	−0.0/-1.7	C10–C12–C14–C15	−180.0/-177.5
C4–C14–C15–O1	−179.5/-175.7	C12–C14–C15–O1	0.5/5.1
C4–C14–C15–C16	0.6/5.2	C12–C14–C15–C16	−179.5/-173.9
O1–C15–C16–C19	0.1/-1.7	C14–C15–C16–C19	−179.9/177.3
C22–N2–C19–C16	−97.4/-87.0	C26–N2–C19–C16	78.2/89.2
C15–C16–C19–N2	179.5/179.6	C24–N3–C22–N2	−0.2/-0.1
C26–N2–C22–N3	0.3/0.2	C19–N2–C22–N3	176.6/177.0
C22–N3–C24–C26	0.0/-0.1	N3–C24–C26–N2	0.2/0.1
C22–N2–C26–C24	−0.3/-0.2	C19–N2–C26–C24	−176.6/-177.1

4. Results and discussion

4.1. IR and raman spectra

The calculated (scaled) wave numbers, observed IR, Raman bands and assignments are given in Table 2 and in the following discussion, the phenyl ring is designated as PhI and imidazole ring as PhII. The bands observed at 1675 cm^{-1} in the IR spectrum, 1672 cm^{-1} in the Raman spectrum and at 1671 cm^{-1} (DFT) are assigned as the stretching modes of the carbonyl (C=O) group. According to literature, the stretching mode of the C=O group is expected in the range 1850–1550 cm^{-1} [28]. The in-plane and out-of-plane bending modes of the C=O group are reported in the ranges 725 ± 95 and 595 ± 120 cm^{-1} [29]. For the title compound, the C=O deformation bands are theoretically assigned at 616, 560 cm^{-1} (DFT).

The stretching and deformation modes of the CH_2 groups appear in the regions 3020–2875, 1480-725 cm^{-1}, respectively [29–31]. The CH_2 stretching modes are observed at 2965, 2921 cm^{-1} in the IR spectrum, 2999, 2965, 2944, 2918 cm^{-1} in the Raman spectrum and theoretically in the range 3008–2919 cm^{-1}. The deformation modes of the CH_2 groups are assigned at 1444, 1415, 1366, 1294, 1269, 1252 cm^{-1} in the IR spectrum, 1444, 1415, 1370, 1351, 1270 cm^{-1} in the Raman spectrum and at 1441, 1418 (scissoring), 1362, 1355 (wagging), 1296, 1267 (twisting), 1254, 1132 (rocking) cm^{-1} theoretically as expected [29–31].

For phenyl rings, the C–H stretching modes are expected above 3000 cm^{-1} [29]. In the title compound, the phenyl CH streching modes are theoretically assigned in the range 3079–3042 cm^{-1}. Experimentally, these bands are observed at 3060 cm^{-1} in the IR and at 3068 cm^{-1} in Raman spectrum. The phenyl ring stretching modes are assigned at 1575 cm^{-1} (IR), 1580 cm^{-1} (Raman) and in the range 1579–1308 cm^{-1} (DFT). The sixth phenyl ring stretching mode, the ring breathing vibration appears as a weak band near 1000 cm^{-1} in mono-, 1-3-di- and 1,3,5-tri substituted benzenes [29,32]. In the present case, the PED analysis gives ring breathing mode at 1009 cm^{-1} for the phenyl ring [29]. The C–H deformation modes of the phenyl ring, in-plane and out-of-plane modes are expected above and below 1000 cm^{-1}, respectively [29]. The in-plane CH deformation bands of the phenyl ring are observed at 1063, 1013 cm^{-1} in the IR spectrum, 1285, 1161, 1139, 1066 cm^{-1} in the Raman spectrum and theoretically in the range 1283–1010 cm^{-1}. The CH out-of-plane deformation modes are assigned at 907, 825 cm^{-1} in the IR spectrum, 905, 827 cm^{-1} in the Raman spectrum and theoretically in the range 969–727 cm^{-1}. The ring substituent deformation modes are also identified and assigned (Table 2) and most of the modes are not pure but contains significant contributions from other modes.

For the title compound, the imidazole ring stretching modes are observed at 1329, 1092, 997 cm^{-1} in the IR spectrum, 1328 cm^{-1} in the Raman spectrum and theoretically at 1479, 1472, 1331, 1097, 998 cm^{-1}. This is in agreement with the work of Almajan et al. [33]. Sandhyarani et al. reported the C–N stretching mode at 1319 cm^{-1} [34]. Benzon et al. reported the imidazole ring, C–N stretching modes at 1247, 1129, 938 cm^{-1} theoretically, 1248, 1135, 926 cm^{-1} in the Raman spectrum and 924 cm^{-1} in the IR spectrum [13]. The C–N stretching modes are reported at 1268, 1220, 1151 cm^{-1} theoreticaly for benzimidazolium salts by Malek et al. [35]. The C=N stretching modes were reported in the range 1535–1666 cm^{-1} [36], 1592 cm^{-1} experimentally and theoretically at 1584 cm^{-1} [37]. For an imidazole derivative, the C=N stretching mode is theoeretically assigned at 1464 cm^{-1}, 1462 cm^{-1} in the IR spectrum and at 1464 cm^{-1} in the Raman spectrum [13]. The C_{19}–N_2 mode is observed at 1212 cm^{-1} in the IR spectrum, 1209 cm^{-1} in the Raman spectrum and theoretically at 1214 cm^{-1} for the title compound.

4.2. Nonlinear optical properties (NLO)

Hyperpolarizabilities are very sensitive to the employed basis set and level of theoretical approach [38–40] because the electron correlation can change the value of hyperpolarizability. Urea is one of the prototypical molecules used in the study of the nonlinear properties of molecular systems. Therefore, it has been frequently used as a threshold value for comparative purposes. The calculations of the total molecular dipole moment, linear polarizability and first order hyperpolarizability from the Gaussian output have been previously explained in detailed [41] and DFT has been extensively used an effective method to investigate the organic NLO material [42]. The polar properties of the title compound were calculated by the density functional theory using the B3LYP method with 6 − 311 ++ G(d) (5D, 7F) basis set using the Gaussian09 program prackage. The calculated first hyperpolarizability of the title compound is 2.209 × 10^{-30} e.s.u, which is 16.99 times that of

Table 2
Calculated (scaled) wavenumbers, observed IR, Raman bands and assignments of the title compound.

B3LYP/6 − 311 ++ G(d) (5D,7F)			IR	Raman	Assignments[a]
υ(cm^{-1})	IR_I	R_A	υ(cm^{-1})	υ(cm^{-1})	-
3134	3.71	107.96	3131	3133	υCHII(98)
3110	3.34	94.90	3111	3112	υCHII(99)
3108	5.33	42.83	–	–	υCHII(98)
3079	7.20	135.56	–	–	υCHI(96)
3071	12.13	169.13	–	3068	υCHI(94)
3062	25.38	76.37	3060	–	υCHI(93)
3052	8.37	123.15	–	–	υCHI(96)
3042	0.23	46.53	–	–	υCHI(94)
3008	8.79	27.14	–	2999	υCH$_2$(97)
2966	14.17	76.41	2965	2965	υCH$_2$(98)
2947	3.44	33.54	–	2944	υCH$_2$(96)
2919	12.08	84.19	2921	2918	υCH$_2$(99)
1671	193.14	75.13	1675	1672	υC = O(80)
1579	28.50	123.96	1575	1580	υPhI(57), δCHI(18)
1560	12.56	10.86	–	–	υPhI(65), δCHI(19)
1479	34.42	3.71	–	–	υCNII(32), υCCII(25), δCHII(29)
1472	32.62	10.74	–	–	υCCII(24), δCHII(23), υCNII(17), δCH$_2$(14)
1469	9.48	3.68	–	–	δCHI(15), υPhI(55)
1441	11.99	5.76	1444	1444	δCH$_2$(76)
1426	25.30	5.44	–	–	δCHI(21), υPhI(69)
1418	4.60	8.62	1415	1415	δCH$_2$(86)
1362	53.40	8.02	1366	1370	δCH$_2$(53), υCNII(23)
1355	43.31	5.53	–	1351	δCH$_2$(53), υCNII(20)
1331	1.30	45.05	1329	1328	υCNII(59), υCCII(13), δCHII(10)
1308	9.75	3.98	–	–	δCHI(15), υPhI(63)
1296	48.76	2.48	1294	–	δCH$_2$(47), υPhI(27)
1283	9.63	0.64	–	1285	υPhI(15), δCH$_2$(17), δCHI(48)
1267	19.87	9.66	1269	1270	δCH$_2$(41), υCNII(13), δCHII(18)
1254	12.49	12.13	1252	–	δCHII(31), δCH$_2$(23), υCN(12), υCNII(14)
1214	26.11	5.69	1212	1209	δCHII(35), υCNII(11), υCN(47)
1178	126.24	39.58	1175	1180	υCC(33), δCH$_2$(18), δCHI(17)
1159	53.86	8.23	–	1161	δCHI(69)
1142	3.36	6.61	–	1139	δCHI(77), υPhI(17)
1132	1.36	2.09	–	–	δCH$_2$(65), υCNII(22)
1097	18.87	5.96	1092	–	υCNII(64), δCHII(27)
1067	3.41	1.52	1063	1066	υPhI(23), δCHI(55)
1054	28.16	11.07	–	–	δCHII(60), υCCII(28)
1034	7.34	13.79	1036	1034	υCC(55), δCH$_2$(19)
1010	7.56	6.68	1013	–	δCHI(46), υCNII(11), δCH$_2$(14)
1009	9.93	23.06	–	1005	υPhI(35), δPhII(10), δCH$_2$(15)
998	8.14	3.32	997	–	υCNII(44), δCH$_2$(36), δPhII(15)
979	5.49	41.86	979	977	δPhI(66), υPhI(19)
969	0.23	0.04	–	–	γCHI(81), τPhI(14)
950	57.24	2.35	–	–	υCC(45), δ_C = O(11), υPhI(10)
948	0.60	0.02	–	–	γCHI(89)
905	1.26	0.09	907	905	γCHI(82)
883	9.69	1.46	–	–	δPhII(82)
824	0.43	0.04	825	827	γCHI(97)
817	2.59	1.52	–	–	γCHII(81), τPhII(13)
804	0.49	14.82	–	803	δCH$_2$(25), υCC(39), δPhII(10)
781	1.66	0.34	–	–	δCH$_2$(46), γC = O(13), τPhI(10)
770	32.76	0.62	–	–	γCHII(79), τPhII(18)
727	48.08	0.28	–	–	τPhI(30), γCHI(40), δCH$_2$(16)
694	1.98	1.50	–	705	δPhI(29), δPhII(14), υCC(30)
689	34.08	1.58	691	–	γCHII(96)
674	38.80	0.01	671	670	τPhI(62), γCHI(30)
647	17.53	0.09	–	642	τPhII(95)
616	37.10	3.11	620	617	δ_C = O(41), δPhI(14), τPhII(20)
611	3.47	0.37	–	–	τPhII(66), δPhI(11), γCN(10)
607	1.14	5.69	–	–	δPhI(72)
560	6.70	0.06	562	565	γC = O(38), γCC(11), τPhI(17)
470	4.53	1.46	474	–	δCC(52), δCH$_2$(21)
412	0.59	0.12	411	416	τPhI(60), γCC(19), γC = O(10)
396	0.01	0.01	–	395	τPhI(83)
379	0.52	1.74	–	–	δCH$_2$(24), δ_C = O(17), δPhI(24)
325	1.08	0.49	–	–	δCN(71)
274	5.53	1.50	–	–	δCC(46), δCH$_2$(20)
216	6.68	1.89	–	–	δCH$_2$(33), δCC(34)
153	0.11	2.66	–	157	γCC(31), τPhI(31),τCH$_2$(15), γC = O(10)
138	0.87	0.58	–	–	γCN(41), δCC(38), δCH$_2$(12)
92	0.58	0.11	–	–	τCN(27), τCH$_2$(38), τC = O(18)
61	6.35	0.41	–	–	τC = O(30), τCH$_2$(40),τCN(12)
50	2.23	3.02	–	–	γCN(35), δCH$_2$(40), δCC(10)

Table 2 (*continued*)

B3LYP/6 – 311 ++ G(d) (5D,7F)			IR	Raman	Assignments[a]
υ(cm^{-1})	IR_I	R_A	υ(cm^{-1})	υ(cm^{-1})	-
30	0.41	4.20	–	–	τC = O(46), τCH_2(40)
28	1.80	7.14	-	-	τCN(50), τCH_2(37)

[a] υ-stretching; δ-in-plane deformation; γ-out-of-plane deformation; τ-torsion; PhI-Phenyl ring; PhII-imidazole ring; potential energy distribution (%) is given in brackets in the assignment column.

standard NLO material urea (0.13×10^{-30} e.s.u) [43]. The average second hyperpolarizability is $\langle\gamma\rangle = (\gamma_{xxxx} + \gamma_{yyyy} + \gamma_{zzzz} + 2\gamma_{xxyy} + 2\gamma_{xxzz} + 2\gamma_{yyzz})/5$. The theoretical second order hyperpolarizability was calculated using the Gaussian09 software and is equal to -11.614×10^{-37} e.s.u [44]. Accordingly, we conclude that the title compound is an attractive object for future studies of nonlinear optical properties.

4.3. Natural bond orbital analysis (NBO)

The natural bond orbitals (NBO) calculations were performed using the NBO 3.1 program [45] as implemented in the Gaussian09 package at the DFT/B3LYP level in order to understand various second-order interactions between the filled orbitals of one subsystem and vacant orbitals of another subsystem, which is a measure of the intermolecular delocalization or hyper conjugation. In NBO analysis, large stabilization energy E(2) value shows the intensive interaction between electron-donors and electron-acceptors, and greater the extent of conjugation of the whole system, the possible intensive interaction are given in Table 3. The second-order perturbation theory analysis of Fock-matrix in NBO basis shows strong intra-molecular hyper-conjugative interactions are formed by orbital overlap between n(O), n(N) and σ*(C–N), π*(C–N), σ*(C–O), π*(C–O), bond orbitals which result in intra-molecular charge transfer causing stabilization of the system. The important intra-molecular hyper-conjugative interactions are $n_2(O_1) \rightarrow \sigma^*(C_{15}–C_{16})$, $n_1(N_2) \rightarrow \pi^*(N_3–C_{22})$ and $n_1(N_3) \rightarrow \sigma^*(N_2–C_{22})$ with stabilization energies 21.23, 47.50 and 9.31 kJ/mol and electron densities 0.05940e, 0.38144e, and 0.04196e. The NBO analysis also describes the bonding in terms of the natural hybrid orbital $n_2(O_1)$, which occupy a higher energy orbital (−0.26945 a.u.) with considerable p-character (100%) and low occupation number (1.88831) and the other $n_1(O_1)$ occupy a lower energy orbital (−0.69024 a.u.) with p-character (43.37%) and high occupation number (1.97778). Thus, a very close to pure p-type lone pair orbital participates in the electron donation to the $n_2(O_1) \rightarrow \sigma^*(C_{15}–C_{16})$, $n_1(N_2) \rightarrow \pi^*(N_3–C_{22})$ and $n_1(N_3) \rightarrow \sigma^*(N_2–C_{22})$ interactions in the compound. The results are tabulated in Table 4.

4.4. Frontier molecular orbital analysis

The HOMO (highest occupied molecular orbital) and LUMO (lowest unoccupied molecular orbital) energy gap of the title compound has been calculated at the B3LYP/6 – 311 ++ G(d) (5D,7F) level. These orbitals determine the way the molecule interacts with other species. Fig. 4 shows the distributions and energy levels of HOMO and LUMO orbitals computed at the B3LYP level for the title compound. The HOMO is mainly localized on the imidazole ring, CH_2 and carbonyl groups. The LUMO is mainly delocalized in the CH_2 group, carbonyl group and the phenyl ring. This shows a charge transfer from the imidazole ring to the phenyl ring through the methylene and carbonyl groups. The value of the energy

Table 3
Second-order perturbation theory analysis of Fock matrix in NBO basis corresponding to the intra-molecular bonds of the title compound.

Donor(i)	Type	ED/e	Acceptor(j)	Type	ED/e	E(2)[a]	E(j)-E(i)[b]	F(ij)[c]
N2–C22	σ	1.98634	N2–C19	σ*	0.02693	1.76	1.14	0.040
_		–	N2–C26	σ*	0.02244	2.04	1.26	0.045
N3–C22	π	1.86756	C24–C26	π*	0.01866	21.54	0.33	0.078
C14–C15	σ	1.98023	C4–C6	σ*	0.01523	1.99	1.24	0.044
_	–	–	C4–C14	σ*	0.02284	2.13	1.23	0.046
_	–	–	C10–C12	σ*	0.01446	2.25	1.25	0.047
_	–	–	C12–C14	σ*	0.02166	1.84	1.23	0.042
_	–	–	C16–C19	σ*	0.01883	1.29	1.03	0.033
C15–C16	σ	1.98354	N2–C19	σ*	0.02693	2.42	0.99	0.044
_	–	–	C12–C14	σ*	0.02166	2.12	1.21	0.045
C16–C19	σ	1.98194	C14–C15	σ*	0.06484	2.44	1.05	0.046
C24–C26	σ	1.98579	N2–C19	σ*	0.02693	5.14	1.04	0.065
_	π	1.86234	N3–C22	π*	0.38144	14.95	0.28	0.061
LPO1	σ	1.97778	C14–C15	σ*	0.06484	1.86	1.12	0.041
_	–	–	C15–C16	σ*	0.05940	1.50	1.07	0.036
_	π	1.88831	C14–C15	σ*	0.06484	19.61	0.70	0.106
_		–	C15–C16	σ*	0.05940	21.23	0.65	0.106
LPN2	σ	1.55450	N3–C22	π*	0.38144	47.50	0.28	0.104
_		–	C16–C19	σ*	0.01883	6.41	0.62	0.063
_		–	C24–C26	π*	0.30939	31.60	0.29	0.089
LPN3	σ	1.92739	N2–C22	σ*	0.04196	9.31	0.82	0.078
-		-	C24–C26	σ*	0.01866	5.61	0.95	0.066

[a] E(2) means energy of hyper-conjugative interactions (stabilization energy in kJ/mol).
[b] Energy difference (a.u) between donor and acceptor i and j NBO orbitals.
[c] F(i,j) is the Fock matrix elements (a.u) between i and j NBO orbitals.

Table 4
NBO results showing the formation of Lewis and non-Lewis orbitals.

Bond(A-B)	ED/e[a]	EDA%	EDB%	NBO	s%	p%
σN2-C22	1.98634	64.49	35.51	$0.8031(sp^{2.00})N+$	33.38	66.62
_	−0.79862	–	–	$0.5959(sp^{2.32})C$	30.12	69.88
πN3-C22	1.86756	56.87	43.13	$0.741(sp^{1.00})N+$	0.00	100.0
_	−0.28527	–	–	$0.6567(sp^{1.00})C$	0.00	100.0
σC14-C15	1.98023	52.11	47.89	$0.7219(sp^{2.25})C+$	30.80	69.20
_	−0.66455	–	–	$0.6920(sp^{1.80})C$	35.64	64.36
σC15-C16	1.98354	48.02	51.98	$0.6930(sp^{1.90})C+$	34.49	65.51
_	−0.64285	–	–	$0.7210(sp^{2.81})C$	26.23	73.77
σC16-C19	1.98194	50.65	49.35	$0.7117(sp^{2.63})C+$	27.51	72.49
_	−0.62329	–	–	$0.7025(sp^{2.55})C$	28.18	71.82
σC24-C26	1.98579	48.64	51.36	$0.6974(sp^{1.73})C+$	36.56	63.44
_	−0.69421	–	–	$0.7167(sp^{1.63})C$	38.02	61.98
πC24-C26	1.86234	48.30	51.70	$0.6950(sp^{1.00})C+$	0.00	100.0
_	−0.25205	–	–	$0.7190(sp^{1.00})C$	0.00	100.0
n1O1	1.97778	–	–	$sp^{0.76}$	56.63	43.37
_	−0.69024					
n2O1	1.88831	–	–	$sp^{1.00}$	0.00	100.00
_	−0.26945					
n1N2	1.55450	–	–	$sp^{99.99}$	0.09	99.01
_	−0.24958					
n1N3	1.92739	–	–	$sp^{2.00}$	33.26	66.74
-	−0.34085	-	-	-	-	-

[a] ED/e in a.u.

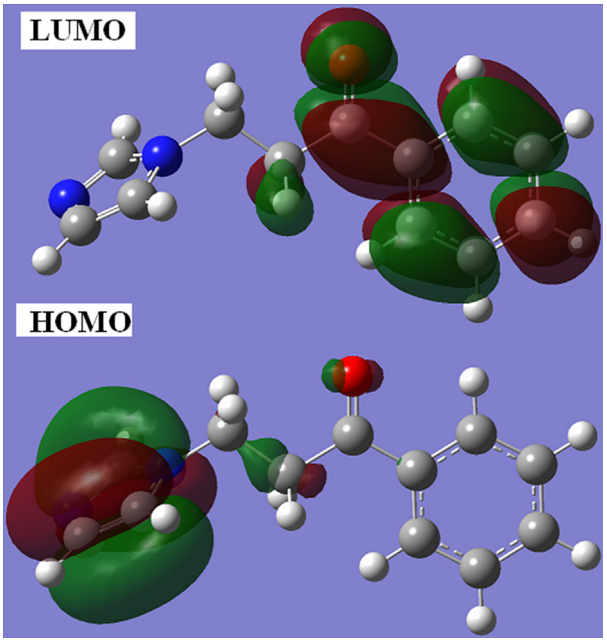

Fig. 4. HOMO-LUMO plots of 3-(1*H*-imidazol-1-yl)-1-phenylpropan-1-one.

separation between the HOMO and LUMO is 3.222 eV. The lowering of the HOMO-LUMO band gap is essentially a consequence of the large stabilization of the LUMO due to the strong electron-acceptor ability of the electron-acceptor group. Using HOMO and LUMO orbital energies, the ionization energy and electron affinity can be expressed as: $I = -E_{HOMO}$, $A = -E_{LUMO}$ [46]. The hardness η and chemical potential μ are given the following relations $\eta = (I-A)/2$ and $\mu = -(I + A)/2$, where I and A are the first ionization potential and electron affinity of the chemical species [46]. For the title compound, the $E_{HOMO} = -8.662$ eV, $E_{LUMO} = -5.440$ eV, Energy gap = HOMO-LUMO = 3.222 eV, Ionization potential I = 8.662 eV, Electron affinity A = 5.440 eV, global hardness η = 1.611 eV, chemical potential μ = −7.051 eV and the global electrophiliciy $= \mu^2/2\eta = 15.430$ eV. It could be concluded that the chemical potential of the title compound is negative and it indicates that the compound is stable.

4.5. Molecular electrostatic potential (MEP)

Molecular electrostatic potential at a point in the space around a molecule gives an indication of the net electrostatic effect produced at that point by the total charge distribution of the molecule and correlates with dipole moments, electronegativity, partial charges and chemical reactivity of the molecules [47]. It provides a visual method to understand the relative polarity of the molecule. The different values of the electrostatic potential at the MEP surface are represented by different colours: red, blue and green represent the regions of most negative, most positive and zero electrostatic potential, respectively. The negative electrostatic potential corresponds to an attraction of the proton by the aggregate electron density in the molecule (shades of red), while the positive electrostatic potential corresponds to the repulsion of the proton by the atomic nuclei (shade of blue). The negative (red and yellow) regions of the MEP were related to the electrophilic reactivity and the positive (blue) regions to the nucleophilic reactivity. From the MEP plot (Fig. 5), it is evident that the negative charge covers the carbonyl group and the nitrogen atom N_3 of the imidazole ring and the positive region is over the remaining portions of the molecule.

4.6. Molecular docking

In addition to the well-documented antifungal activity of imidazole derivatives, several imidazole and fused imidazole structures are associated with a wide range of biological activities including antiviral [48], anticancer [49,50], antitrypanosomal [51], antimalarial [52–54], antihistaminic [55] and anticoagulant [56] activities. Thus, it was of interest to study the molecular docking of the title molecule as an inhibitor of *plasmodium falciparum*, the causative agent of malaria. High resolution crystal structure of *plasmodium falciparum* was downloaded from the protein data bank website (PDB ID: 3PBL) and all molecular docking calculations were performed on AutoDock-Vina software [57]. The 3D crystal structure of *plasmodium falciparum* was obtained from the Protein Data Bank and the protein was prepared for docking by removing the co-crystallized ligands, water and co-factors and the Auto Dock Tools (ADT) graphical user interface was used to calculate the Kollman charges and polar hydrogens. The ligand was prepared for docking by minimizing its energy at the B3LYP/6 − 311 ++ G(d) (5D,7F) level of theory and the partial charges were calculated by Geistenger method. The active site of the enzyme was defined to

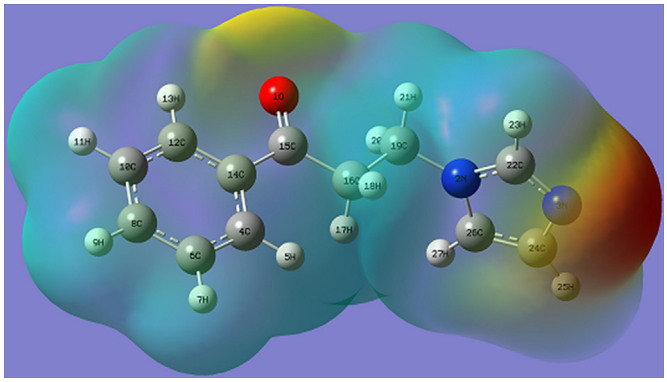

Fig. 5. MEP plot of 3-(1*H*-imidazol-1-yl)-1-phenylpropan-1-one.

include the residues of the active site within the grid size of 40 Å × 40 Å × 40 Å and the most popular algorithm, Lamarckian Genetic Algorithm (LGA) available in Autodock was employed for docking and the docking protocol was tested by extracting co-crystallized inhibitor from the protein and then docking the same. The docking protocol predicted the same conformation as was present in the crystal structure with RMSD value well within the reliable range of 2 Å [58]. Amongst the docked conformations, one which binds well at the active site was analyzed for detailed interactions in Discover Studio Visualizer 4.0 software. The ligand binds at the active site of the substrate (Figs. 6 and 7) by weak non-covalent interactions. The amino acids Phe202, Tyr167 shows π-π interaction with the phenyl ring and Asn165, Gln203 forms H–bond interaction with the C═O group and imidazole ring, respectively. The docked ligand title compound forms a stable complex with *plasmodium falciparum* and gives a binding affinity (ΔG in kcal/mol) value of −5.5 (Table 5). These preliminary results suggest that the compound might exhibit antimalarial activity against *plasmodium falciparum* (Fig. 8).

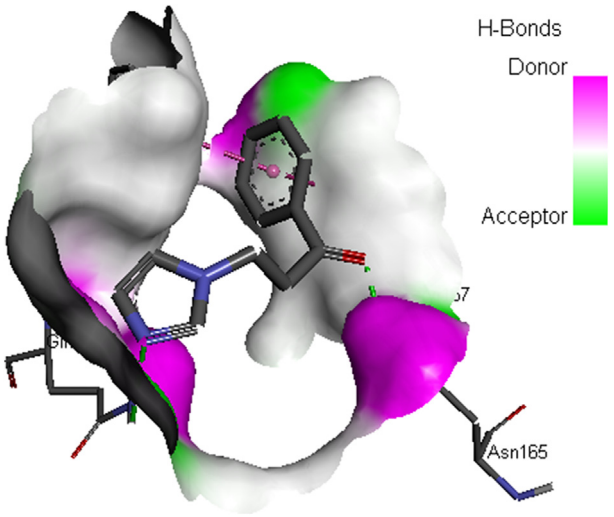

Fig. 7. The docked protocol reproduced the co-crystallized conformation with H-bond (green), π-anion (brown), alkyl (pink) and H-bond receptor surface.(For interpretation of the references to colour in this figure legend, the reader is referred to the web version of this article.)

4.7. Geometrical parameters

In the title compound, the carbon–carbon bond lengths (DFT/XRD) in the phenyl ring lie in the range 1.3927–1.4026/1.3762–1.3937 Å and these values are somewhere in between the normal values for a single (1.54 Å) and a double (1.33 Å) bond [59]. The C_{22}–N_3 bond length (DFT/XRD) = 1.3141/1.3098 Å shows typical double bond characteristics. However, the C_{24}–N_3 = 1.3747/1.3622, C_{26}–N_2 = 1.3812/1.3612, C_{22}–N_2 = 1.3672/1.3445 bond lengths (DFT/XRD) are shorter than the normal C–N single bond length of about 1.48 Å, while the reported corresponding values are 1.407, 1.395, 1.3874 Å [60] and 1.4176, 1.4001, 1.391 Å [13]. At N_2 position, the bond angles (DFT/XRD) are C_{26}–N_2–C_{22} = 106.2/106.0, C_{26}–N_2–C_{19} = 126.9/126.9 and C_{22}–N_2–C_{19} = 126.8/127.0° and this asymmetry in angles reveal the steric repulsion between the imidazole ring and adjacent CH_2 groups. The imidazole ring is tilted from the adjacent methylene groups, as is evident from the torsion angles, C_{24}–C_{26}–N_2–C_{19} = −176.6, C_{26}–N_2–C_{19}–C_{16} = 78.2, N_3–C_{22}–N_2–C_{19} = 176.6 and C_{22}–N_2–C_{19}–C_{16} = −97.4°.

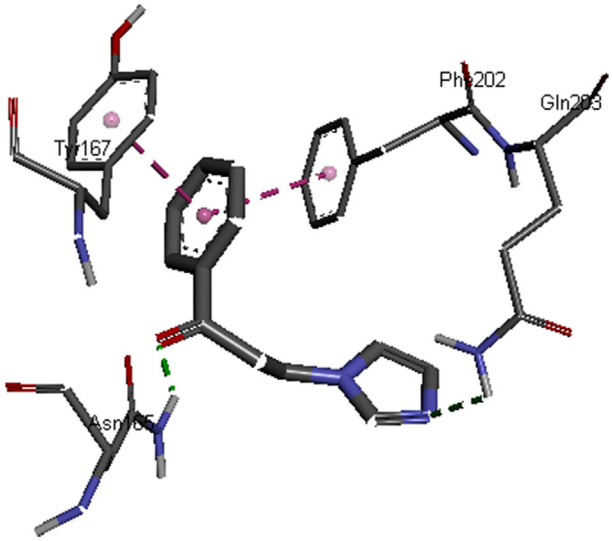

Fig. 6. Schematic presentation of the interaction of dopamine D3 receptor and ligand.

Table 5
The binding affinity values of different poses of the title compound predicted by AutodockVina.

Mode	Affinity (kcal/mol)	Distance from best mode (Å)	
_	_	RMSD l.b.	RMSD u.b.
1	−5.5	0.000	0.000
2	−5.2	2.584	3.287
3	−5.1	26.737	28.337
4	−5.1	3.207	4.036
5	−5.0	2.719	3.638
6	−5.0	1.520	2.180
7	−5.0	22.820	26.244
8	−5.0	3.923	5.431
9	−5.0	2.749	4.733

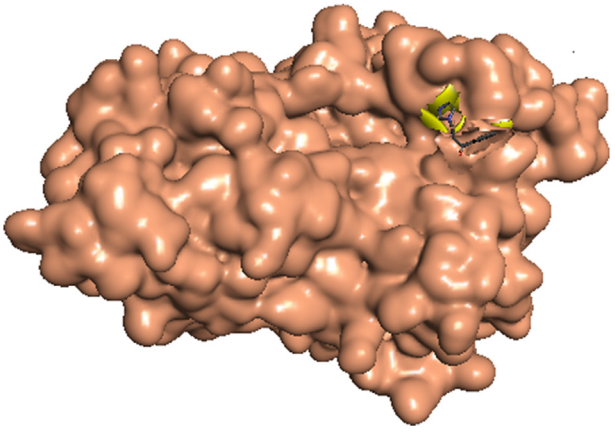

Fig. 8. Pictorial representation of the ligand embedded in the active site of human dopamine D3 receptor.

5. Conclusions

The vibrational spectroscopic studies of 3-(1*H*-imidazol-1-yl)-1-phenylpropan-1-one were reported theoretically and experimentally. Potential energy distribution of normal modes of vibrations

was done with the help of GAR2PED software. The HOMO is mainly localized on the imidazole ring, CH_2 and carbonyl groups and the LUMO is mainly delocalized in the CH_2 group, carbonyl group and the phenyl ring and the lowering of the HOMO-LUMO energy gap supports for the bioactivity of the molecule. MEP predicts the most reactive part in the molecule and from the MEP plot, it is evident that the negative charge covers the carbonyl group and the nitrogen atom N_3 of the imidazole ring and the positive region is over the remaining portions of the molecule. The first and second hyperpolarizability values are also reported and the title compound is a good object for further studies in nonlinear optics. From the molecular docking study, the ligand binds at the active site of the substrate by weak non-covalent interactions and the amino acids Phe202, Tyr167 shows π-π interaction with the phenyl ring and Asn165, Gln203 forms H–bond interaction with the C═O group and imidazole ring, respectively.

Acknowledgements

The authors would like to extend their sincere appreciation to the Deanship of Scientific Research at King Saud University for funding this work through the Research Group Project No. PRG-1436-23.

References

[1] S.K. Fridkin, W.R. Jarvis, Clin. Microbiol. Rev. 9 (1996) 499–511.
[2] J.R. Wingard, H. Leather, Biol. Blood Marrow Transpl. 10 (2004) 73–90.
[3] M.A. Pfaller, D.J. Diekema, Crit. Rev. Microbiol. 36 (2010) 1–53.
[4] W. Wang, C. Sheng, X. Che, H. Ji, Z. Miao, J. Yao, W. Zhang, Arch. Pharm. Chem. Life Sci. 342 (2009) 732–739.
[5] J.T. Slama, J.L. Hancock, T. Rho, L. Sambucetti, K.A. Bachmann, Biochem. Pharmacol. 55 (1998) 1881–1892.
[6] H. Ji, W. Zhang, M. Zhang, M. Kudo, Y. Aoyama, Y. Yoshida, C. Sheng, Y. Song, S. Yang, Y. Zhou, J. Med. Chem. 46 (2003) 474–485.
[7] B. Narasimhan, D. Sharma, P. Kumar, Med. Chem. Res. 20 (2011) 1119–1140.
[8] D.J. Sheehan, C.A. Hitchcock, C.M. Sibley, Clin. Microbiol. Rev. 12 (1999) 40–79.
[9] M.A. Hossain, M.A. Ghannoum, Exp. Opin. Invest. Drugs 9 (2000) 1797–1813.
[10] M.N. Aboul-Enein, A.A. El-Azzouny, M.I. Attia, O.A. Saleh, A.L. Kansoh, Arch. Pharm. Chem. Life Sci. 344 (2011) 794–801.
[11] M.I. Attia, A.A. Radwan, A.S. Zakaria, M.S. Almutairi, S.W. Ghoneim, Chem. Cent. J. 7 (2013) 168.
[12] M.I. Attia, A.S. Zakaria, M.S. Almutairi, S.W. Ghoneim, Molecules 18 (2013) 12208–12221.
[13] K.B. Benzon, H.T. Varghese, C.Y. Panicker, K. Pradhan, B.K. Tiwary, A.K. Nanda, C. Van Alsenoy, Spectrochim. Acta A 151 (2015) 965–979.
[14] N. Sundaraganesan, S. Ilakiamani, P. Subramani, B.D. Joshua, Spectrochim. Acta A 67 (2007) 628–635.
[15] K.B. Benzon, H.T. Varghese, C.Y. Panicker, K. Pradhan, B.K. Tiwary, A.K. Nanda, C. Van Alsenoy, Spectrochim. Acta A 146 (2015) 307–322.
[16] S.A. Laufer, W. Zimmermann, K.J. Ruff, J. Med. Chem. 47 (2004) 6311–6325.
[17] Ö. Uçucu, N.G. Karaburun, Í. Işkdağ, Farmaco 56 (2001) 285–290.
[18] C.A. Hamilton, Pharmacol. Ther. 54 (1992) 231–248.
[19] M.I. Attia, H.A. Ghabbour, A.A. El-Azzouny, O.A. Al-Deeb, M.S. Almutairi, H.-K. Fun, J. Chem. 2013 (2013) 1–5. Article ID 515309.
[20] Gaussian 09, Revision B.01, M.J. Frisch, G.W. Trucks, H.B. Schlegel, G.E. Scuseria, M.A. Robb, J.R. Cheeseman, G. Scalmani, V. Barone, B. Mennucci, G.A. Petersson, H. Nakatsuji, M. Caricato, X. Li, H.P. Hratchian, A.F. Izmaylov, J. Bloino, G. Zheng, J.L. Sonnenberg, M. Hada, M. Ehara, K. Toyota, R. Fukuda, J. Hasegawa, M. Ishida, T. Nakajima, Y. Honda, O. Kitao, H. Nakai, T. Vreven, J.A. Montgomery, Jr., J.E. Peralta, F. Ogliaro, M. Bearpark, J.J. Heyd, E. Brothers, K.N. Kudin, V.N. Staroverov, T. Keith, R. Kobayashi, J. Normand, K. Raghavachari, A. Rendell, J.C. Burant, S.S. Iyengar, J. Tomasi, M. Cossi, N. Rega, J.M. Millam, M. Klene, J.E. Knox, J.B. Cross, V. Bakken, C. Adamo, J. Jaramillo, R. Gomperts, R.E. Stratmann, O. Yazyev, A.J. Austin, R. Cammi, C. Pomelli, J.W. Ochterski, R.L. Martin, K. Morokuma, V.G. Zakrzewski, G.A. Voth, P. Salvador, J.J. Dannenberg, S. Dapprich, A.D. Daniels, O. Farkas, J.B. Foresman, J.V. Ortiz, J. Cioslowski, D.J. Fox, Gaussian, Inc., Wallingford CT, 2010.
[21] W. Kohn, L.J. Sham, Phys. Rev. A140 (1965) 1133–1138.
[22] A.D. Becke, J. Chem, Phys. 98 (1993) 5648–5652.
[23] B.K. Paul, N. Guchhait, Comput. Theor. Chem. 1012 (2013) 20–26.
[24] C. Lee, W. Yang, R.G. Parr, Phys. Rev. B37 (1988) 785–789.
[25] N.C. Handy, P.E. Masley, R.D. Amos, J.S. Andrews, C.W. Murray, G. Laming, Chem. Phys. Lett. 197 (1992) 506–515.
[26] R. Dennington, T. Keith, J. Millam, GaussView, Version 5, Semichem Inc., Shawnee Mission, KS, 2009.
[27] J.M.L. Martin, C.V. Alsenoy, GAR2PED, a Program to Obtain a Potential Energy Distribution from a Gaussian Archive Record, University of Antwerp, Belgium, 2007.
[28] G. Socrates, Infrared Characteristic Group Frequencies, John Wiley and Sons, New York, 1981.
[29] N.P.G. Roeges, A Guide to the Complete Interpretation of Infrared Spectra of Organic Structures, John Wiley and Sons Inc., New York, 1994.
[30] N.B. Colthup, L.H. Daly, S.E. Wiberly, Introduction to Infrared and Raman Spectroscopy, Academic Press, New York, 1990.
[31] R.M. Silverstein, F.X. Webster, Spectrometric Identification of Organic Compounds, 6th, John Wiley Asia, 2003.
[32] G. Varsanyi, Assignments of Vibrational Spectra of Seven Hundred Benzene Derivatives, Wiley, New York, 1974.
[33] G.L. Almajan, S.F. Barbuceanu, L. Farcasanau, C. Draghici, Rev. Chim. Buchar. 62 (2011) 386–390.
[34] N. Sandhyarani, G. Skanth, S. Berchmanns, V. Yegnaraman, T. Pradeep, J. Colloid Interface Sci. 209 (1999) 154–161.
[35] K. Malek, A. Puc, G. Schroeder, V.I. Rybachenko, L.M. Proniewich, Chem. Phys. 327 (2006) 439–451.
[36] S. Genç, N. Dege, A. Çetin, A. Cansiz, M. Sekerci, M. Dinçer, Acta Cryst. E60 (2004) o1580.
[37] H. Tanak, Y. Köysal, Y. Ünver, M. Yavuz, Ş. Işik, K. Sanck, Mol. Phys. 108 (2010) 127–139.
[38] A.E. Reed, L.A. Curtiss, F. Weinhold, Chem. Soc. 102 (1988) 899–926.
[39] J.P. Foster, F. Weinhold, J. Am. Chem. Soc. 102 (1980) 7211–7218.
[40] H. Sekino, R.J. Bartlett, J. Chem. Phys. 84 (1986) 2726–2733.
[41] J. Henriksson, T. Saue, P. Norman, J. Chem. Phys. 128 (2008) 105–112.
[42] J.P. Hermann, D. Ricard, J. Ducuing, Appl. Phys. Lett. 23 (1973) 178–180.
[43] C. Adant, M. Dupuis, J.L. Bredas, Int. J. Quantum. Chem. 56 (2004) 497–507.
[44] C. Hätting, O. Christiansen, P. Jørgensen, Chem. Phys. Lett. 282 (1998) 139–149.
[45] E.D. Glendening, A.E. Reed, J.E. Carpenter, F. Weinhold, NBO Version 3.1, Gaussian Inc., Pittsburgh, PA, 2003.
[46] R.J. Parr, R.G. Pearson, J. Am. Chem. Soc. 105 (1983) 7512–7516.
[47] S. Sebastian, N. Sundaraganesan, Spectrochim. Acta A 75 (2010) 941–952.
[48] C.A. Dvorak, R. Apodaca, A.J. Barbier, C.W. Berridge, S.J. Wilson, J.D. Boggs, W. Xiao, T.W. Lovenberg, N.I. Carruthers, J. Med. Chem. 48 (2005) 2229–2238.
[49] J. Chen, S. Ahn, J. Wang, Y. Lu, J.T. Dalton, D.D. Miller, W. Li, J. Med. Chem. 55 (2012) 7285–7289.
[50] R. Wang, C. Chen, X. Zhang, C. Zhang, Q. Zhong, G. Chen, Q. Zhang, S. Zheng, G. Wang, Q.-H. Chen, J. Med. Chem. 58 (2015) 4713–4726.
[51] G. Andriani, E. Amata, J. Beatty, Z. Clements, B.J. Coffey, G. Courtemanche, W. Devine, J. Erath, C.E. Juda, Z. Wawrzak, J.T. Wood, G.I. Lepesheva, A. Rodriguez, M.P. Pollastri, J. Med. Chem. 56 (2013) 2556–2567.
[52] L. Zhang, R. Sathunuru, D. Caridha, B. Pybus, M.T. O'Neil, M.P. Kozar, A.J. Lin, J. Med. Chem. 54 (2011) 6634–6646.
[53] A.M. Sanz, F. Gómez-Contreras, P. Navarro, M. Sánchez-Moreno, S. Boutaleb-Charki, J. Campuzano, M. Pardo, A. Osuna, C. Cano, M.J.R. Yunta, L. Campayo, J. Med. Chem. 51 (2009) 1962–1966.
[54] G.N. Vazquez, M.D.M.R. Vilchis, L.Y. Mulia, V. Melendez, L. Gerena, A.H. Campos, R. Castillo, F.H. Lui, Eur. J. Med. Chem. 41 (2006) 135–141.
[55] M. Govoni, R.A. Bakker, I. van de Wetering, M.J. Smit, W.M.B.P. Menge, H. Timmerman, S. Elz, W. Schunack, R. Leurs, J. Med. Chem. 46 (2003) 5812–5824.
[56] J.J. Hangeland, T.J. Friends, K.A. Rossi, J.M. Smallheer, C. Wang, Z. Sun, J.R. Corte, T. Fang, P.C. Wong, A.R. Rendina, F.A. Barbera, J.M. Bozarth, J.M. Luettgen, C.A. Watson, G. Zhang, A. Wei, V. Ramamurthy, P.E. Morin, G.S. Bisacchi, S. Subramaniam, P. Arunachalam, A. Mathur, D.A. Seiffert, R.R. Wexler, M.L. Quan, J. Med. Chem. 57 (2014) 9915–9932.
[57] O. Trott, A.J. Olson, J. Comput. Chem. 31 (2010) 455–461.
[58] B. Kramer, M. Rarey, T. Lengauer, Proteins Struct. Funct. Genet. 37 (1999) 228–241.
[59] P. Sykes, A Guide Book to Mechanism in Organic Chemistry, sixth ed., Pearson Education, India, New Delhi, 2004.
[60] Y.S. Mary, P.J. Jojo, C.Y. Panicker, C. Van Alsenoy, S. Ataei, I. Yildiz, Spectrochim. Acta A 122 (2014) 499–511.